Anomalous Spin-Resolved Point-Contact Transmission of Holes due to Cubic Rashba Spin-Orbit Coupling

Stefano Chesi,[1,2,3] Gabriele F. Giuliani,[1] L. P. Rokhinson,[1] L. N. Pfeiffer,[4] and K. W. West[4]

[1]Department of Physics, Purdue University, West Lafayette, Indiana 47907, USA
[2]Department of Physics, University of Basel, 4056 Basel, Switzerland
[3]Department of Physics, McGill University, Montreal, Quebec, Canada H3A 2T8
[4]Department of Electrical Engineering, Princeton University, Princeton, New Jersey 08544, USA

(Received 11 November 2010; published 10 June 2011)

Evidence is presented for the finite wave vector crossing of the two lowest one-dimensional spin-split subbands in quantum point contacts fabricated from two-dimensional hole gases with strong spin-orbit interaction. This phenomenon offers an elegant explanation for the anomalous sign of the spin polarization filtered by a point contact, as observed in magnetic focusing experiments. Anticrossing is introduced by a magnetic field parallel to the channel or an asymmetric potential transverse to it. Controlling the magnitude of the spin splitting affords a novel mechanism for inverting the sign of the spin polarization.

DOI: 10.1103/PhysRevLett.106.236601 PACS numbers: 72.25.−b, 71.70.Ej, 73.23.Ad, 85.75.−d

The control of spin-dependent transport in semiconductors is a central theme of fundamental and technological relevance [1,2]. For holes, strong effects of the spin-orbit coupling have been observed in low-dimensional structures [2–7], and interest in the transport properties of quantum point contacts (QPCs) has also been spurred by investigations of the so-called 0.7 anomaly [8–10]. In such hole QPCs, an intriguing and still unexplained observation is the anomalous sign of the spin polarization revealed by magnetic focusing experiments [4,8,9,11].

It is well known that an asymmetric potential confining electrons or holes in 2D generates an intrinsic spin-orbit interaction (the so-called Rashba effect [12]). However, the resulting spin-orbit coupling is very different in the two cases: for holes it is approximately cubic in momentum instead of being linear as for electrons [2,3]. We show here that the presence of cubic Rashba spin-orbit coupling explains the anomalous sign in the QPC transmission and, based on this, we suggest how to control the sign of the spin polarization.

Our magnetic focusing devices are fabricated from a high mobility ($\sim 0.4 \times 10^6$ V $\cdot$ s/cm^2) shallow 2D hole gas [13] using an atomic force microscopy (AFM) local anodic oxidation technique; see inset in Fig. 1(a). The devices consist of two QPCs oriented along the $[33\bar{2}]$ crystallographic direction, with lithographical distance $L = 0.8$ μm between their centers. The actual distance is smaller due to large repulsive voltages on the side gates (~ 0.2 V) and attractive on the center gate (-0.3 V). Conductance of both QPCs and the nonlocal focusing signal was measured using standard ac lock-in techniques with excitation current 1 nA at a base temperature $T = 25$ mK. The focusing signal $V_{\rm foc}$ is defined as the voltage across the detector QPC in response to the current flowing through the injector QPC; see [4,9] for details. In the presence of perpendicular magnetic field $B < 0$, Shubnikov–de Haas (SdH) oscillations in the adjacent 2D gas are observed, see Fig. 1(a), and the measured hole density is $p = 1.45 \times 10^{11}$ cm^{-2}. For $B > 0$ several peaks due to magnetic focusing are superimposed onto the SdH oscillations. When the conductance of both QPCs is tuned

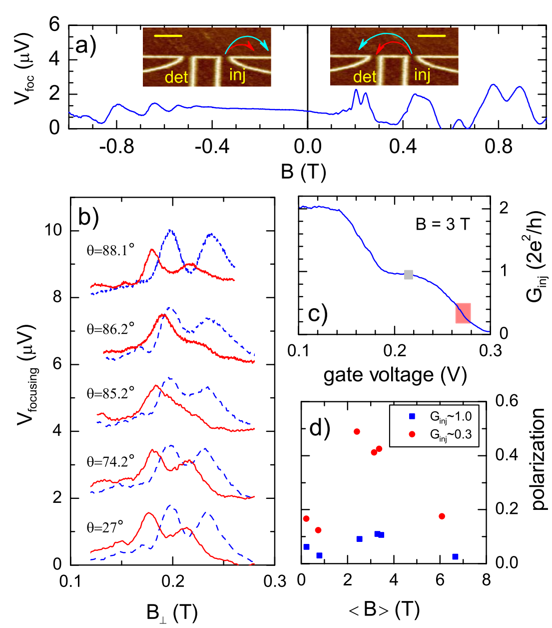

FIG. 1 (color online). (a) Voltage across the detector QPC as a function of magnetic field for zero tilt angle. Insets: AFM micrograph of a sample, where arrows schematically show the cyclotron motion for the two spin orientations; the bars are 0.5 μm scales. (b) Signal for the first focusing peak in a tilted magnetic field. Curves are offset for clarity. The values of $G_{\rm inj}$ for dashed blue (solid red) curves are within the smaller (larger) rectangles in the injector QPC characteristic in (c). (d) Relative population of the spin subbands, estimated for $G_{\rm inj} = 2e^2/h$ (blue squares) and $G_{\rm inj} \sim 0.3 \times 2e^2/h$ (red dots).

to be $2e^2/h$, the first focusing peak splits into two peaks. If the conductance of the injector QPC is $G_{\text{inj}} < 2e^2/h$, the rightmost peak is slightly suppressed, which has been interpreted as spontaneous polarization [8].

Applying $B_\parallel$ along $[33\bar{2}]$ affects the energies of the spin subbands without affecting the cyclotron motion. Experimentally this is achieved by tilting the sample. The focusing data in a tilted magnetic field are plotted in Fig. 1(b) [14]. When $G_{\text{inj}} = 2e^2/h$, no filtering is expected and, indeed, both focusing peaks have approximately the same height as at $\theta = 0$. With the increase of the tilt angle, the Zeeman splitting of the spin subbands in a 2D gas increases. For $G_{\text{inj}} < 2e^2/h$ preferential transmission of the largest k_F spin subband is expected for electrons, which corresponds to a suppression of the *left* peak. Instead, in a hole gas we observe suppression of the *right* peak up to $\theta \approx 85°$ ($B_\parallel \approx 2.5$ T); see Fig. 1(b). For $\theta > 85°$ the right peak reappears. The data are summarized in Fig. 1(d), where polarization $P = (V_{\text{left}} - V_{\text{right}})/(V_{\text{left}} + V_{\text{right}})$ is plotted as a function of the total field $\langle B\rangle = (B_{\text{right}} + B_{\text{left}})/2$, averaged between the positions of the two peaks, with V_{left} and V_{right} focusing signals for the left and right peaks [9].

The anomalous behavior of P cannot be explained with linear Rashba spin-orbit coupling (see [11] for a theoretical analysis). On the other hand, as we will show, it naturally follows from the Rashba spin-orbit coupling for 2D holes, of the form $\frac{i\gamma}{2}(\hat{p}_-^3\hat{\sigma}_+ - \hat{p}_+^3\hat{\sigma}_-)$ [2,3]. Here, $\hat{p}_\pm = \hat{p}_x \pm i\hat{p}_y$ and $\hat{\sigma}_\pm = \hat{\sigma}_x \pm i\hat{\sigma}_y$, with $\hat{\boldsymbol{\sigma}}$ the Pauli matrices. Such cubic spin-orbit interaction is responsible for a peculiar dispersion of the lowest two 1D subbands. For a channel with lateral extent W, aligned with the x axis, we can substitute $\langle p_y^2\rangle \sim (\hbar\pi/W)^2$ and $\langle p_y\rangle \sim 0$ in the 2D Hamiltonian, which gives

$$\hat{H}_{1\text{D}} = \frac{\hat{p}_x^2}{2m} + \gamma\left(\frac{3\hbar^2\pi^2}{W^2}\hat{p}_x - \hat{p}_x^3\right)\hat{\sigma}_y + \frac{\hbar^2\pi^2}{2mW^2}. \qquad (1)$$

Because of the lateral confinement, a linear spin-orbit coupling term appears in Eq. (1), which is dominant at small momenta but coexists with a cubic contribution with opposite sign. Therefore, the spin subbands cross not only at $k_x = 0$ but also at the finite wave vectors $k_x = \pm\sqrt{3}\pi/W$. This is at variance with the Rashba spin-orbit splitting for electrons, which is monotonically increasing (linear in momentum) both in 2D and 1D.

To confirm Eq. (1), we solved the 3D problem in the framework of the Luttinger Hamiltonian. We take into account the full cubic symmetry and consider a quantum well with growth direction [113], as in the experiment. An electric field $\mathcal{E}_z$ along the confinement direction produces Rashba spin-orbit coupling and the energy splitting is $\sim k^3$ in 2D. We then introduce a lateral confinement potential and obtain 1D subbands, plotted in Fig. 2. For simplicity, we choose hard wall confining potentials. The 1D bands clearly display the main feature we are interested in: the presence of a crossing point at finite wave vector. We also checked that bulk-inversion asymmetry terms [2,15] only introduce minor modifications in Fig. 2 and that by setting $\mathcal{E}_z = 0$ a small spin splitting survives, which, however, does not induce crossing of the lowest two 1D subbands. For this reason, we have neglected the Dresselhaus spin-orbit terms [6] in the effective 2D and 1D Hamiltonians.

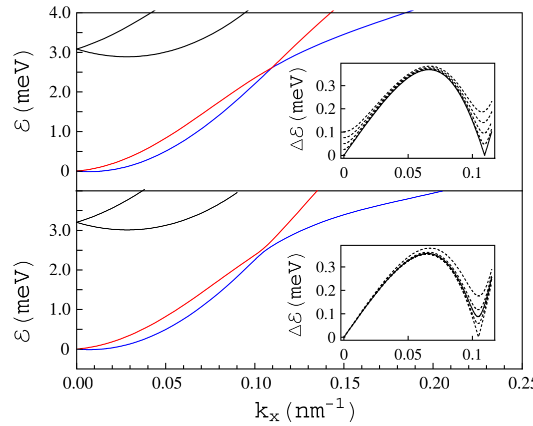

FIG. 2 (color online). Energy subbands of 1D channels obtained from a 15 nm quantum well grown in the [113] direction. An electric field $\mathcal{E}_z = 1$ V/μm along [113] is present. The lateral confinement has width $W = 40$ nm. Upper panel: Wire along $[33\bar{2}]$. The inset shows the energy splitting of the two lowest subbands at several values of $B_\parallel$. The solid curve is for $B_\parallel = 0$ and the dashed curves for $B_\parallel = 0.5, 1, 1.5, 2$ T. Lower panel: Wire along $[1\bar{1}0]$. The inset shows the energy splitting with a lateral electric field. The solid curve is for $\mathcal{E}_y = 0$ and the dashed curves for $\mathcal{E}_y = \pm 12.5, \pm 37.5$ V/mm (the splitting is reduced for positive values of $\mathcal{E}_y$).

As seen in the inset of Fig. 2 (top panel), the degeneracies at $k_x = 0$ and finite k_x are removed when $B_\parallel \neq 0$. Within the effective Hamiltonian (1), the external magnetic field is taken into account by adding a Zeeman term $g^*\mu_B B_\parallel\hat{\sigma}_x/2$, where g^* is the effective g factor [5] and μ_B the Bohr magneton. The total effective magnetic field, which includes the spin-orbit interaction, depends on the values of W and k_x as follows:

$$\vec{B}_{\text{eff}}(W, k_x) = B_\parallel\hat{x} + \frac{2\gamma\hbar^3}{g^*\mu_B}\left(\frac{3\pi^2}{W^2}k_x - k_x^3\right)\hat{y}, \qquad (2)$$

where $\hat{x}, \hat{y}$ are unit vectors along the coordinate axes. The eigenstates of Eq. (1), $\psi_W(k_x, \pm) = e^{ik_x x}|k_x, \pm\rangle_W$, have spinor functions $|k_x, \pm\rangle_W$ parallel or antiparallel to $\vec{B}_{\text{eff}}$ and energies

$$\epsilon_\pm(W, k_x) = \frac{\hbar^2k_x^2}{2m} \mp \frac{1}{2}g^*\mu_B|\vec{B}_{\text{eff}}(W, k_x)|. \qquad (3)$$

At $k_x = 0$ and $k_x = \pm\sqrt{3}\pi/W$ the spin splitting is $g^*\mu_B B_\parallel$; i.e., it is only due to the external magnetic field.

In a realistic QPC the width $W(x)$ of the lateral confinement changes along the channel. As in [16] we assume a sufficiently smooth variation of the width, such that the holes adiabatically follow the lowest *orbital* subband. Introducing in Eq. (1) the x-dependent width $W(x) = W_0 e^{x^2/2\Delta x^2}$, where Δx is a typical length scale of the QPC and W_0 its minimum width, we obtain the following effective Hamiltonian:

$$\frac{\hat{p}_x^2}{2m} + V(\hat{x}) + \frac{g^* \mu_B}{2} B_\parallel \hat{\sigma}_x + \gamma[3m\{V(\hat{x}), \hat{p}_x\} - \hat{p}_x^3]\hat{\sigma}_y,$$

with $\{a, b\} = ab + ba$ [17]. The potential barrier has the following form:

$$V(x) = \frac{\hbar^2 \pi^2}{2mW(x)^2} = \frac{\hbar^2 \pi^2}{2mW_0^2} e^{-x^2/\Delta x^2}, \tag{4}$$

As it will be presently made clear, the main qualitative conclusions are independent of the detailed form of the potential, but Eq. (4) allows us to solve explicitly the 1D transmission problem and obtain the spin-resolved conductance in the Landauer-Büttiker formalism. The scattering eigenstates are obtained with incident wave functions $\psi_{W=\infty}(k_\mu, \mu)$ at $x \ll -\Delta x$, where $\mu = \pm$ denotes the spin subband and $k_\pm$ are determined by the Fermi energy ϵ_F, at which the holes are injected in the QPC. For $x \gg \Delta x$, such QPC wave functions have the asymptotic form $\sum_{\nu=\pm} t_{\mu,\nu} \psi_\infty(k_\nu, \nu)$, where $t_{\mu,\nu}$ are transmission amplitudes. The spin-resolved conductances are simply given by $G_\pm = \frac{e^2}{h} \sum_{\mu=\pm} \frac{v_\pm}{v_\mu} |t_{\mu,\pm}|^2$ [18], where the Fermi velocities are $v_\pm = \frac{\partial \epsilon_\pm(\infty, k_\pm)}{\partial \hbar k_x}$, from Eq. (3). The total conductance is $G = G_+ + G_-$. Typical results at several values of $B_\parallel$ are shown in Fig. 3. As usual, by opening the QPC, a current starts to flow above a minimum value of W_0. The spin polarization behaves as follows.

(i) At $B_\parallel = 0$ T we obtain a structureless unpolarized conductance ($G_+ = G_-$), but we find $G_- > G_+$ at larger values of the magnetic field (see the top right panel of Fig. 3, at $B_\parallel = 3$ T); i.e., the holes in the *higher* spin subband have larger transmission at the first plateau. The sign is opposite to the case of linear Rashba spin-orbit coupling (see [11]) and in agreement with the experimental results of Fig. 1.

(ii) At $B_\parallel \approx 7$ T (see the bottom left panel of Fig. 3), $G_+ \simeq G_-$ and the transmission becomes unpolarized, as observed in the data of Fig. 1.

(iii) At even larger values of $B_\parallel > 7$ T, we obtain $G_+ \simeq e^2/h$, $G_- \simeq 0$ (bottom right panel of Fig. 3). Although this regime is yet to be experimentally investigated, this represents a natural prediction of our theory: at sufficiently large magnetic field the role of the spin-orbit coupling becomes negligible and the spin direction (parallel or antiparallel to the external magnetic field) of the holes is conserved. The injected holes remain in the original ("+" or "−") branch and the current at the first plateau is polarized in the "+" band, which has lower energy. Deviations from this behavior are due to nonadiabatic transmission in the spin subbands, and, to gain a qualitative understanding, we consider next a semiclassical picture of the holes.

When a hole wave packet is at position x, it is subject to a magnetic field $\vec{B}_{\rm eff}$ determined by $W(x)$ and $k_x(x)$ as in Eq. (2). For holes injected at ϵ_F, the momentum is determined by energy conservation. Treating the spin-orbit coupling as a small perturbation compared to the kinetic energy, we have $k_x(x) \simeq \sqrt{k_F^2 - \pi^2/W(x)^2}$, where $k_F = \sqrt{2m\epsilon_F}/\hbar$ is the Fermi wave vector in the absence of spin-orbit coupling. Therefore, the injected hole experiences a varying magnetic field in its semiclassical motion along x, due to the change of both k_x and $W(x)$. For adiabatic transmission of the spin subbands the spin follows the direction of the magnetic field, but this is not possible in general if $B_\parallel$ is sufficiently small. In particular, for $B_\parallel = 0$ Eq. (1) implies that $\hat{\sigma}_y$ is conserved. Therefore, the initial spin orientation along y is not affected by the motion of the hole. On the other hand, $\vec{B}_{\rm eff}$ of Eq. (2) changes direction when $k_x = \sqrt{3}\pi/W$ and $B_\parallel = 0$. After this point, a hole in the "+" branch continues its motion in the "−" branch and vice versa.

At finite in-plane magnetic field the degeneracy of the spectrum is removed but the holes do not follow adiabatically the spin branch, unless the Landau-Zener condition $\frac{dB_y/dt}{B_\parallel} \ll \omega_B$ is satisfied, where $\hbar\omega_B = g^* \mu_B B_\parallel$. The change ΔB_y in the spin-orbit field is obtained from Eq. (2): $|B_y|$ is equal to $2\gamma\hbar^3 k_F^3/g^* \mu_B$ far from the QPC and vanishes at the degeneracy point. This change occurs on the length scale Δx of the QPC and we can estimate the time interval with $\Delta t \simeq \Delta x/v$ where v is a typical velocity of the hole. This gives

$$B_\parallel \gg \sqrt{\frac{\hbar \Delta B_y}{g^* \mu_B \Delta t}} \simeq \frac{\hbar^2 \sqrt{2\gamma k_F^3 v/\Delta x}}{g^* \mu_B}. \tag{5}$$

To estimate v at the degeneracy point $k_x = \sqrt{3}\pi/W$, we solve $\sqrt{3}\pi/W \simeq \sqrt{k_F^2 - \pi^2/W^2}$ to obtain $k_x = \frac{\sqrt{3}}{2} k_F$.

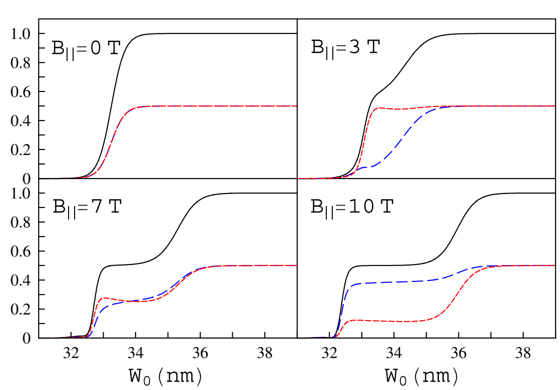

FIG. 3 (color online). Total conductance G (black solid curves) and spin-resolved conductances G_+ (blue, long-dashed curves) and G_- (red, short-dashed curves), plotted in units of $2e^2/h$ as functions of the minimum width W_0 of the QPC [see Eq. (4)]. We used parameters appropriate for the experimental setup: $m = 0.14m_0$ [20], where m_0 is the bare electron mass, $g^* = 0.8$ [5], $\gamma\hbar^3 = 0.45$ eV nm^3, $\Delta x = 0.3$ μm, and $\epsilon_F = 2.3$ meV.

Therefore, v is large at the degeneracy point ($v \simeq v_F$, where $v_F = \hbar k_F/m$ is the Fermi velocity), and to follow adiabatically the spin branches requires a large external field. The crossover occurs for

$$B^* \simeq \frac{(\hbar k_F)^2\sqrt{2\gamma\hbar/(m\Delta x)}}{g^*\mu_B}. \quad (6)$$

This expression gives $B^* \simeq 7.4$ T with the parameters of Fig. 3, in agreement with the more accurate numerical analysis. Below B^*, holes injected in the "+" band cross nonadiabatically to the "−" spin branch when $k_x \simeq \sqrt{3}\pi/W$. Therefore, holes injected in the lower subband have higher energy at $x \simeq 0$ and are preferentially reflected, as seen in the top right panel of Fig. 3 with $B_\parallel = 3$ T. The reflection is not perfect, due to nonadiabaticity at $k_x \simeq 0$: at this second quasidegenerate point the "−" holes can cross back to the "+" branch and be transmitted. We attribute to this effect the enhanced conductivity $G > e^2/h$ at the first conductance plateau in the top right panel of Fig. 3, while a well-defined e^2/h plateau is obtained at larger magnetic field. In fact, the adiabatic approximation becomes accurate at $k_x \simeq 0$ for smaller values of $B_\parallel$ [19] than B^*.

The above discussion makes it clear that the degeneracy of the hole spectrum at $k_x = \sqrt{3}\pi/W$ is crucial to obtain the anomalous transmission of Figs. 1 and 3. The special behavior we have described cannot be realized with linear Rashba spin-orbit coupling [11]. Furthermore, Eq. (6) allows us to predict how the value of the crossover field can be controlled. A lower value of B^* can be obtained with a smaller coupling γ, a smoother QPC (i.e., larger Δx), or a lower hole gas density (i.e., smaller k_F). The value of the Fermi wave vector has a large influence, since it contributes both to the spin splitting $\gamma\hbar^3k_F^3$ and to the velocity v_F of the holes.

It is also remarkable that the degeneracy of the 1D spectrum at finite k_x is removed for a channel oriented along the $[1\bar{1}0]$ direction, as shown in the bottom panel of Fig. 2. The reason is that the lateral confinement is along the low symmetry direction $[33\bar{2}]$ and the mirror symmetry of the channel is broken by the crystalline potential. At the anticrossing, we obtain a ~0.1 meV splitting (see inset). For the other orientation of the wire this splitting corresponds to a magnetic field $B_\parallel \sim 1$ T, and it is therefore quite sizable. This also suggests that it should be possible to modify the spin splitting, and thus the crossover field B^*, via electric gates. We consider in the second inset of Fig. 2 an electric field $\mathcal{E}_y$ in the transverse direction of the channel and obtain that the splitting can be either reduced or increased by varying $\mathcal{E}_y$. In contrast to the case $B_\parallel \neq 0$, the degeneracy at $k_x = 0$ is not lifted by the transverse electric field.

In conclusion, we have shown that the cubic Rashba spin-orbit coupling for holes provides an explanation of the anomalous sign of the spin polarization observed in QPCs in 2D hole gases. The theory nicely explains the presence of a crossover field B^* at which the transmission is unpolarized, predicts that above B^* a polarization in the lowest spin subband is recovered, and indicates how the value of B^* can be modified.

We would like to thank Yu. Lyanda-Geller and E. I. Rashba for useful discussions. S. C. acknowledges support by NCCR Nanoscience, Swiss NSF, and CIFAR.

[1] *Semiconductor Spintronics and Quantum Computation*, edited by D. D. Awschalom, D. Loss, and N. Samarth (Springer, New York, 2002).
[2] R. Winkler, *Spin-Orbit Coupling Effects in Two-Dimensional Electron and Hole Systems* (Springer, Berlin, 2003).
[3] R. Winkler, Phys. Rev. B **62**, 4245 (2000); R. Winkler *et al.*, Phys. Rev. B **65**, 155303 (2002); S. Chesi and G. F. Giuliani, Phys. Rev. B **75**, 155305 (2007).
[4] L. P. Rokhinson *et al.*, Phys. Rev. Lett. **93**, 146601 (2004).
[5] R. Danneau *et al.*, Phys. Rev. Lett. **97**, 026403 (2006); S. P. Koduvayur *et al.*, *ibid.* **100**, 126401 (2008).
[6] D. V. Bulaev and D. Loss, Phys. Rev. Lett. **95**, 076805 (2005); M. Trif, P. Simon, and D. Loss, Phys. Rev. Lett. **103**, 106601 (2009).
[7] C. H. L. Quay *et al.*, Nature Phys. **6**, 336 (2010).
[8] L. P. Rokhinson, L. N. Pfeiffer, and K. W. West, Phys. Rev. Lett. **96**, 156602 (2006).
[9] L. P. Rokhinson, L. N. Pfeiffer, and K. W. West, J. Phys. Condens. Matter **20**, 164212 (2008).
[10] Y. Komijani *et al.*, Europhys. Lett. **91**, 67 010 (2010).
[11] A. Reynoso, G. Usaj, and C. A. Balseiro, Phys. Rev. B **75**, 085321 (2007).
[12] Y. A. Bychkov and E. I. Rashba, J. Phys. C **17**, 6039 (1984).
[13] L. P. Rokhinson, D. C. Tsui, L. N. Pfeiffer, and K. W. West, Superlattices Microstruct. **32**, 99 (2002).
[14] The shift seen in Fig. 1(b) between traces at the same tilt angle can be attributed to a local decrease of hole density from the side gates (0.22 V for the blue dashed traces and 0.265–0.28 V for the red solid traces).
[15] E. I. Rashba and E. Ya. Sherman, Phys. Lett. A **129**, 175 (1988).
[16] L. I. Glazman *et al.*, JETP Lett. **48**, 238 (1988).
[17] The anticommutator is introduced to obtain a Hermitian Hamiltonian. This has negligible effect in the limit of a smooth contact when $\partial V/\partial x$ is small.
[18] We define $G_\pm$ with unpolarized incident holes and spin-resolved detection. The conductances for spin-polarized holes and unpolarized detection have the same values of $G_\pm$ in our model.
[19] Using $v = 3\gamma(\hbar\pi/W_0)^2 \simeq 3\gamma(\hbar k_F)^2$ [as obtained from Eq. (3) at $k_x = 0$ and $x = 0$], Eq. (5) gives $B \gg 3.5$ T.
[20] A. Meney, Superlattices Microstruct. **11**, 387 (1992); T. Minagawa, Ph.D. thesis, Purdue University, 2010.